Fundamental Conical Defects: the d-Cone, its e-Cone and its "p-Cone"

Keith A. Seffen

kas14@cam.ac.uk

Advanced Structures Group Laboratory, Department of Engineering, University of Cambridge, UK, CB2 1PZ

June 22, 2016

Abstract

We consider well-known surface disclinations by cutting, joining and folding pieces of paper card. The resulting shapes have a discrete, folded vertex whose geometry is described easily by Gauss's mapping, in particular, we can relate the degree of angular excess, or deficit, to the size of fold-line rotations by the area enclosed by the vector diagram of these rotations. This is well known for the case of a so-called "d-Cone" of zero angular deficit, and we formulate the same for a general disclination. This method allows us to observe kinematic properties in a meaningful way without needing to consider equilibrium. Importantly, the simple vector nature of our analysis shows that some disclinations are primitive; and that other types, such as d-Cones, are amalgamations of them.

1 Introduction

Surface *disclinations* are associated with a rapid change in the orientation, or rotation, of a surface, usually along a straight line; a *dislocation* occurs when there is a jump in positional order [1]. Disclinations are typically formed by first adding or subtracting material from *within* an originally flat surface. If the surface is very thin, this change in material content is accommodated by elastic, out-of-plane bending in preference to in-plane straining according to Gauss's *Theorema Egregium* [2]: and, in structural terms, equilibrium must be satisfied in this deformed or *buckled* state whilst respecting the support conditions.

Figure 1 shows how this behaviour can be achieved using a disk of ordinary paper card. The disk has been cut radially towards its centre before being splayed into a flat, open wedge of around 15°. Later, we insert extra card for continuity, to form a positive disclination, but we note for now that the split edges have to be held down by adhesive tape, Fig. 1(a). Approximately two-thirds of the disk lie naturally flat without surface fixity; the remainder has lifted off to form a distinctly conical vertex connected to the flat parts by narrow transition zones on each side. As the wedge angle is manually increased, the cone becomes taller but not wider, and the angle subtended around the vertex rises above 360°. Such angular *excess* connotes the term "e-Cone" for this shape [3]. For much larger wedge angles, the width of the cone also changes as more of the disk detaches from the underlying surface because of increasing geometrical nonlinearity: although interesting, this regime is beyond the scope of study.

Properties of e-Cones have been widely studied in recent times in view of, for example, growing biological structures (and material activation in thin plates) [3] and of repeating local features in highly deformed sheets and strips [4]. The angular width of the conical projection has been observed to be independent of material, thickness or wedge angle—if not too great; and this width also depends on how the conical region is defined, whether or not the transition zones

are included. Figures 1(b) and (c) show a repeat of the card experiment using a geometrically nonlinear finite element analysis. Its details are described in the caption and contours of transverse displacement are shown above the level of imperfection needed to induce buckling, which evidently include the transition zones. The conical width is clearly in line with the 120° from our crude card experiment; analytical studies that consider a perfectly flat disk initially, suggest angles closer to 180° [5].

The shape in Fig. 1(a) is mostly *developable* because the paper card is thin, but close to the vertex the surface must be doubly and negatively curved because Gauss's theorem tells us that the angular excess imposed at the vertex produces an exact amount of Gaussian curvature. If we then imagine the card thickness being reduced to zero, the Gaussian curvature becomes concentrated at the vertex tip as a "point charge". The same concentration occurs when the disk is folded instead along three radial lines, in order to emulate the e-Cone in a discrete manner, see Fig. 1(d). These lines are symmetrically located with respect to the radial cut: along the tallest meridian and where the e-Cone of Fig. 1(a) begins to lift off on either side. When the wedge angle is opened horizontally, adjacent plate regions slide on the surface as per the continuum case. The other plates move upwards under fold-line rotations to form approximately the original conically-shaped buckle. The meridian now forms as a ridge, or *mountain* fold, and the lift-off lines as *valley* folds. Assuming that the vertex is perfect and that the plates, or *facets*, remain flat, the folded shape is described entirely by the fold line rotations and the wedge angle. This is a simpler kinematical specification *c.f.* the continuum case without detriment to the accuracy of shape: both e-Cones from Fig. 1 have roughly the same conical widths and wedge angles, with very similar proportions of shape.

Opening the wedge angle right up to when the cone facets become vertical and contact each other, and closing it back to zero, requires little effort when the fold lines are repeatedly flexed for compliancy. The shape, however, becomes more difficult to fold when the valley folds in plan are separated by nearly 180°. At this value and beyond, the disk "locks" and the wedge cannot be opened. This locking is not due to the material stiffening but to inadmissible fold line rotations, as will be shown. When they are separated by more than 180°, folding can proceed only when disk is made to overlap at the cut—when angular *deficit* is imposed at the vertex, and this case is treated momentarily. Otherwise, feasible folded shapes are made stiff by fixing the wedge angle, say, by gluing the open edges to the surface. Extra deformation in this case is promoted by flexibility of the facets alone.

A wedge of material is inserted into the gap of Fig. 1(d) and, by adjusting the fold-line rotations, the folded shape can be seated naturally upright, see Fig. 2(a). If the insertion is repeated for the continuum case and no other forces are applied, the disk will bend everywhere including the wedge itself and attempt to form a "free-standing" e-Cone [3], which displaces upwards and sits above the original surface. Bending of the wedge in this case suggests folding the wedge in the discrete case as an extra mountain fold so that all facets move upwards, Fig. 2(b). As for the simple e-Cone of Fig. 1(d), the valley folds cannot be separated by 180° exactly otherwise folding is impossible: in other words, our free-standing e-Cone must be asymmetrically shaped. Other e-Cones made with more fold lines can, of course, exhibit more symmetrical shapes but our simplified rendition is closest in behaviour to the simplest continuum case of Fig 1(a).

It is possible to recover the first shape of Fig. 2(a) by simply flattening the wedge fold of Fig. 2(b). Furthermore, its folding direction can be reversed to form another valley fold, requiring the disk to be simply supported on a rim as shown in Fig. 2(c). This shape can also be free-standing because the fold lines can be worked into a set of compatible rotations but we show it being held in equilibrium by a central point force—as for the continuum case, which must be forcibly displaced from its free-standing position. The resulting displacement fields of the latter are developable

and conical, and the effect of such *conical confinement* under loads is compared alongside angular (material) excess in [5], in the first study on their interaction. These two variables are specified in [5] only in kinematic terms without recourse to the expediting forces, and the main results are listed shortly; but we impress two further folded shapes in Figs 2(d) and 2(e).

Angular deficit is imposed at the vertex by excising material or by overlapping at the radial cut to form a negative disclination. These shapes are sometimes called "d-Cones" but the literature is not clear on whether or not "d" stands for developable or deficit (or, indeed, disclination): here, we shall assume a d-Cone is a "developable cone" of zero deficit following [10]. In addition to the cut, three fold lines are needed for out-of-plane shaping when the deficit is varied. They must be in the same sense either as valley- or mountain folds, and their layout in plan view is a Y-shape positioned symmetrically with respect to the cut; note that being symmetrical is not essential for planar folding but here it simplifies the problem slightly. The entire disk now folds into a triangular pyramidal cone, Fig. 2(d), which we denote as a "p-Cone". By fixing the angular deficit—by gluing the overlapping parts together, the p-Cone is rendered stiff. Adding a fourth symmetrical fold in the middle of the overlap, Fig. 2(e), imparts mobility *i.e* enables rigid-body motion in the same way as the wedge fold does in the e-Cone of Fig. 2(c). If we imagine the overlapping part (or the inserted wedge) folding by itself, then we locally change the angular deficit (or excess) as if we were shaping the folded disk under compatible fold rotations. Note that both vertices in Figs 2(d) and 2(e) have positive Gaussian curvature.

We aim to consider more carefully the kinematics of our discrete disclinations. As noted, there are already related and successful continuum-based studies, which capture the surface shape via the circumferential variation of radial generators [6, 7] as a governing equation of deformation akin to the well-known beam elastica [8]; the disclination effect usually enters via the boundary conditions. The recent study in [5] concludes that the equilibrium shape of conically confined e-Cones depends only on the ratio of angular excess to the square of conical indentation *i.e.* vertex displacement, and that the effects of conical confinement and Gaussian charge are *interchangeable* for small deflections. They also solve for the conical width as a function of the constraints, and regime maps are furnished accordingly; but they also note that the singular vertex presents solution challenges which may limit the "application of predictions to real sheets".

By deliberately focussing on discretely folded shapes, we are making two points. First, that singular geometrical features are complementary in the analytical sense when we consider point vertices, fold lines and zero thickness facets together. The kinematics are only relevant because we cannot capture equilibrium conditions without appropriate constitutive models for these features, which are being developed in other studies *e.g.* [9]. Second, we wish to emphasise the applicability of our structures directly in practical problems and not just as analogous solutions of the continuum cases. For example, the natural conical widths of e-Cones are largely invariant under small deflections but we allow this width *viz.* the angular separation of the valley folds, to vary so that we may explore a fuller range of symmetrically folded shapes; we may go even further by lifting the symmetry restriction but that is another level of study.

Our analysis is algebraic and solves for fold rotations rather than displacements, which is fortuitous given that disclinations are related to step changes in surface orientation. Moreover, the relationship between angular excess and fold rotations is captured explicitly in a simple Gauss mapping of rotation vectors, which immediately reveals the relative dependencies of shape purported in [5]. We solve first for the behaviour of simple d-Cones without angular excess. This gives a limiting case for confined e-Cones, which are treated afterwards. One surprising feature is that some Gauss mappings can be composed from elements that themselves are fundamental types of disclination: that

these *primitive units* can be combined to make other forms. For example, we show that a d-Cone combines the e-Cone of Fig. 2(a) and the p-Cone of Fig. 2(d). This suggests that real disclinations may obey a similar hierarchy.

2 Discrete d-Cones

A flat disk rests concentrically on a simple rim in Fig. 3(a) and carries a central point force. Conical transverse displacements ensue, where a given radial line rotates downwards about the rim. Simple geometry shows that this leads to in-plane circumferential compression, which cannot be maintained indefinitely. This is relieved by the part of the disk buckling upwards and separating from the rim into the d-Cone mode shape. Although our demonstration is contrived, d-Cones prevail as characteristic "motifs" in many other problems of constrained thin-walled plate deformation [10, 11]. Their geometry for different materials and disk sizes is remarkably consistent, in particular, the lift-off width, which has been the focus of many experiments and analysis. There is reasonable agreement depending on whether or not the width includes the transition regions, which are curved in the opposite sense to the conical bulk—and at what point in the post-buckling phase the width is measured, but typically it subtends $110^\circ - 140^\circ$ in plan view.

Figure 3(b) is a discretely folded d-Cone. The layout of fold lines emanating from the central vertex is similar to the earlier e-Cones of Figs 1 and 2, and is shown in plan view in Fig. 3(c). The pattern also conforms to the rules of vertex folding in origami structures where four symmetrically arranged fold lines meet at the vertex as three valley folds and one mountain fold [12]. This ensures mobility of the folded shape and thus continuous motion up to a point where all facets can "flat-fold" and contact each other in a vertical plane under fold rotations equal to 180°. We shall concern ourselves only with small rotations and deflections that do not alter the fold layout in plan view for the sake of simplicity. The lift-off region extends between the valley folds inclined at angle β on either side of the mountain fold which forms the buckled apex: in Fig. 3(b), $\beta = 60^\circ$, giving a lift-off angle of 120°. The disk is now supported only at three points underneath each valley fold which, for analysis, we set to be at the disk rim of radius, r, even though the disk must overlap the rim in practice.

A side-view of maximal displacements is given in Fig. 3(d) where d_1 is the indentation depth and d_2 is the lift-off height. These evidently arise when the relevant fold lines, shown in true view, rotate by angles, x and y, to the horizontal, giving

$$d_1 = rx, \quad d_2 = ry - rx \tag{1}$$

In order to calculate x and y, we first consider the deformed shape everywhere in terms of *normal vectors* to the disk surface. As these normals rotate away from vertical, we can map them with the same orientation onto the surface of a sphere with unit radius—the *unit sphere*, as proposed by Gauss [2]. Within a given facet, all normals have the same orientation and therefore map to a point on the unit sphere. When we move across a fold, there is a step change in orientation between facets, which traces part of a great arc equal in length to the fold rotation. Following a complete path around the vertex produces a closed figure of fold rotations. For small rotations, the figure is effectively *planar*, and we have constructed, albeit though by a different route, the vector diagram of fold rotations that would be obtained by adding them directly as vectors in the same sequence around the vertex [13]. The mapping for the d-Cone of Fig. 3(b) is now constructed using a positive right-handed screw notation: the rotation vector for a mountain fold points towards the vertex moving in a counter-clockwise sense around it, as shown in Fig. 4(a), and for a valley fold it

points away, Fig. 4(b). Because of the planarity of mapping, maximum fold rotations are of the order of 15° so that the rotations in Fig. 3(d) are much less than unity and the displacements are shallow—but not to the detriment of predicting general behaviour.

The layout of d-Cone fold lines is repeated in Fig. 4(c) with facet labels A to D counter-clockwise, and fold rotations moving from A to B, B to C and so forth as vectors ab, bc *etc*—using the convention from [13]—when drawn in sequence in Fig. 4(d). The Gauss mapping forms a "bow-tie" polygon and, to simplify the notation slightly, we replace ab with γ, bc and da (because of symmetry) with θ, and cd with ϕ. The reason for pursuing Gauss's method becomes apparent because his remarkable theorem asserts that the *area* enclosed by the polygon is equal to the angular deficit at the vertex [2]. The area carries a sign depending on the construction sequence; so, for the left-hand side of Fig. 4(d), the vectors also form counter-clockwise when we move around that side of the vertex in the same sense, giving positive area, whilst in the right-hand side, they form in the opposite clockwise sense, giving negative area. For a d-Cone, however, there is no deficit and thus, the net area must balance. In Fig. 4(d), this requirement sets $\phi = \gamma$ and $\theta = \phi/\cos\beta$. We see immediately that β must be less than 90° for positive values of θ; more importantly, as β approaches this limit, θ increases exponentially outside the realm of small rotations and the d-Cone cannot fold in practice but deforms elastically under the central load. If β is larger than 90°, the Gauss mapping is no longer valid unless the vector, ab, reverses direction. The facets, A and B, would now be connected by a mountain fold and the mapping would be trapezoidal in outline with a net negative area and, hence, angular deficit at the vertex; this is a different physical problem altogether from the d-Cone, so $\beta = 90°$ is a natural upper bound.

Returning to Fig. 4(d), the original rotations, x and y, occur at right angles to the rotations across the fold lines to which they pertain. Therefore, x and y can be drawn as vectors which bisect and lie at right angles to ab and cd, respectively, as shown. They originate from the same point and span the width of the polygon, giving $x + y = \theta \sin\beta$. Their absolute lengths can only be established when support points, P, Q and R, are added to Fig. 4(c). The facets, A and B, also rotate about the lines PQ and PR with equal rotations that, when projected onto the fold line between A and B, sum to ϕ. These extra rotations therefore equal $\phi/[2\cos(\beta/2)]$ and, when multiplied by the lever arm $h = r\sin(\beta/2)$ as shown, yield a vertex displacement, rx. Hence

$$x = \frac{\phi}{2}\tan\frac{\beta}{2}, \quad y = \phi\tan\beta - x; \quad \Rightarrow \quad \frac{d_2}{d_1} = 2\left[\frac{\tan\beta}{\tan\beta/2} - 1\right] \tag{2}$$

For $\beta = 60°$, $d_2/d_1 = 4$, which tallies well with Fig. 3(b). The expression is independent of fold rotations provided they remain small, and it shows that the displacement ratio can increase asymptotically as β approaches 90°, which we observe in other paper card models. Conversely, as β tends to zero—in the limit of the fold lines not overlapping in practice, the displacement ratio approaches two.

3 Discrete e-Cones

We begin with the simplest discrete e-Cone of Fig. 1(d) equivalent to the "planar confined" continuum case, as it is called, in [5]. Recall that the disk opens up along a radial wedge with adjacent facets, A and B, remaining horizontal. We define the angular excess to be the angle, α, subtended by the open wedge in Fig. 5(a). Its magnitude has been exaggerated for clarity, for otherwise, the original plan view of fold lines cannot alter during deformation. There are three folds, and the facets, C and D, move upwards. The Gauss mapping is also drawn in Fig. 5(a) using the same

rules and fold nomenclature used in Fig. 4 with the valley folds having rotation θ and the mountain fold, ϕ. It forms a simple isosceles triangle in which $\theta = \phi/(2\cos\beta)$. The enclosed area is trivial to calculate but we must be mindful of signs because the mapping moves in the opposite direction to the facet sequence in the disk; however, positive area pertains to angular deficit when we have imposed an excess. The area calculation is thus:

$$-\frac{1}{2} \times \frac{\phi}{2} \times \phi \tan\beta = -\alpha \quad \Rightarrow \quad \phi = \sqrt{\frac{4\alpha}{\tan\beta}} \tag{3}$$

The apex displacement, d_2, can be directly computed from multiplying the lever arm to it from either θ-fold line to return

$$d_2 = \frac{\phi}{2\cos\beta} \times r\sin\beta \quad \Rightarrow \quad \frac{d_2}{r} = \sqrt{\alpha\tan\beta} \tag{4}$$

after substituting for ϕ from Eqn 3. For positive values of α, β must lie between 0° and 90°. When β approaches the upper limit, however, ϕ becomes disproportionately large compared to α, and folded displacements are not viable in practice giving way to locking as reported earlier. Conversely, negative values of α *i.e.* angular deficit, would suggest $90° < \beta < 180°$; this is true but we need to be careful about the signs of rotations, which is treated shortly. Note that the square-root presence in Eqn 4 signifies that small changes in small values of α yield relatively larger changes in displacement.

A material wedge subtending the same angle, α, is now added to the disk in Fig. 5(b) with a central valley fold. This is equivalent to the conically confined e-Cone in [5] with facets A and B moving downwards and C and D upwards, the disk being supported at three points on a rim like the d-Cone. The valley fold angle is γ and the Gauss mapping traces an uneven bow-tie—unlike the d-Cone. The θ-fold angle now depends on ϕ and γ according to $\theta = (\phi+\gamma)/(2\cos\beta)$, as does the enclosed area, which is made of two triangular areas of opposite signs. The area calculation is, again, fairly trivial:

$$-\frac{\phi^2}{4\tan\beta} + \frac{\gamma^2}{4\tan\beta} = -\alpha \quad \Rightarrow \quad \phi^2 = \gamma^2 + \frac{4\alpha}{\tan\beta} \quad \textit{i.e.} \quad \frac{\phi^2}{\gamma^2} = 1 + \frac{4\alpha}{\gamma^2\tan\beta} \tag{5}$$

Once more β ranges from 0° to 90° and ϕ in Eqn 3 is recovered when γ is zero.

A side-view of this e-Cone is similar in profile to Fig. 3(d), where it is trivial to show that the maximal displacement ratio depends on the same angles, x and y, using Eqn 1, giving $d_2/d_1 = y/x - 1$. Again, the sum of x and y spans the width of the Gauss mapping, $x + y = \theta\sin\beta$, and again, absolute x is found by considering how the central vertex moves due to rotation about the support lines, returning $x = (\gamma/2)\tan(\beta/2)$. Using this information, we determine:

$$\frac{d_2}{d_1} = \left[\frac{\phi}{\gamma} + 1\right] \frac{\tan\beta}{\tan\beta/2} - 2 \tag{6}$$

Before computing some values, we remark that this ratio depends on the fold angle ratio, ϕ/γ, which in turn depends on α/γ^2 from Eqn 5 for a given value of β. But the indentation depth, x, is proportional to γ, so we see that d_2/d_1 is controlled by the parameter α/x^2, which is precisely the claim made in [5] when we remind ourselves that α is the Gaussian "charge" and x measures the conical confinement.

If we set a parameter, C, equal to α/γ^2, which is similar to α/x^2 except for the contribution from β, we can make the following predictions. When C is small and less than unity, α is small and the displacement ratio approaches the case of the d-Cone, Eqn 2. On the other hand, a large value of C, greater than unity, suggests that γ is small and

we approach the planar confined case of Fig. 5(a) but we never reach it because C becomes infinite. In this case, $\phi/\gamma \approx \sqrt{4C/\tan\beta}$ using Eqn 5, which then becomes the dominant term in Eqn 6:

$$\frac{d_2}{d_1} \approx \frac{\phi}{\gamma}\frac{\tan\beta}{\tan\beta/2} = \frac{2\sqrt{C\tan\beta}}{\tan\beta/2} \tag{7}$$

Equations 2 and 7 are plotted in Fig. 6 alongside the exact expression, Eqn 6, for several values of C. Since C ignores any contribution from β, we can plot everything as functions of β. The limit predictions perform very well and all curves festoon in the sense of d_2/d_1 being large for either small or large values of β, being somewhat flat in between. The absolute minimum value of displacement ratio approaches two, and high ratios (> 10) can be attained, even for low values of C. Thus, by choosing α and β, the "control" range for d_2/d_1 can be very diverse. Note that absolute values d_1 and d_2 can be found easily using Eqn 1 if we wish.

Consider two further shapes in closing this section. In Fig. 5(d), the inserted wedge has a mountain fold as per the free-standing e-Cone of Fig. 2(b). The area enclosed by its Gauss mapping is also given by Eqn 5 even though the direction of γ has reversed (but γ still takes a positive value). We note, however, from the mapping that $\theta = (\phi - \gamma)/(2\cos\beta)$. Hence, if we compare the shapes of free and conical e-Cones with the same α, which both have the same values of ϕ and γ from the area calculation, then the free-standing e-Cone has smaller θ rotations. The "buckled" portion is therefore less elevated in the free case. Constitutive behaviour of the fold lines is not considered here but we can see why the free-standing case has two mountain folds if the strain energy stored is determined by the level of folding: some of the rotations are relatively smaller, less strain energy is stored and thus, it is the preferred equilibrium state. This is speculative, of course, but it matches how both e-Cones "feel" in reality.

In Fig. 5(e), we reproduce the p-Cone fold layout of Fig. 2(d), where the angular deficit, α, of the overlap is a positive value. Since the Gauss mapping moves in the same direction as the facet orientation, then the area calculation reveals that:

$$\frac{1}{2} \times \frac{\gamma}{2} \times \gamma\tan\beta = \alpha \quad \Rightarrow \quad \gamma = \sqrt{\frac{4\alpha}{\tan\beta}} \tag{8}$$

which is exactly the same as the planar e-Cone of Fig. 5(a) and Eqn 3 when ϕ is replaced with γ but only because the fold rotations are in the same sense. Recall that if the sign of α is reversed in Eqn 3 for angular deficit, a negative value of $\tan\beta$ has β in the range 90° to 180°. If this requirement is applied to the layout pattern in Fig. 5(a), then we form the same image as Fig. 5(d) but flipped upside down (and with the original mountain fold becoming a valley fold). Such antisymmetrical behaviour provides alternative insight into general e-Cones, as now discussed.

4 Primitive forms

We return to the d-Cone in Fig. 7. Given that its Gauss mapping equates to the vector diagram of small rotations at the vertex, we can apply the rules of vector manipulation to the mapping—indeed, any mapping. For example, we can divide the bow-tie into two identical triangular halves, which can be recombined to yield the original mapping. But if we compare both halves to Fig. 5, they are respectively the planar e-Cone and the p-Cone, which are redrawn in Fig. 7. The angular excess and deficit at each vertex must cancel in order to produce a d-Cone: in other words, a d-Cone can be formed by adding together a planar e-Cone and a p-Cone with equal and opposite levels of Gaussian charge. In practice, this does not happen; it is merely a different view of how the properties of shape superpose. But it does hint

that we may consider the performance of planar e-Cones, or p-Cones, *by themselves*, in order to understand general disclination cases. Indeed, all of the Gauss mappings presented are a combination of these primitive units of differing Gaussian charges, depending on the net level at the vertex. Consequently, there may be hidden insights afforded by the equivalent continuum cases, particularly the p-Cone, because of its obvious axisymmetry and potentially simpler analysis. We leave this as an exercise in further work.

5 Conclusions

There are excellent and detailed studies on the continuous shape of deformed surfaces around disclinations. We have focused here on developable, folded-plate approximations of the same problem for simplicity's sake, in order to reveal more succinct, if approximate, expressions for the kinematics. We have attempted to frame our results from the same perspective in [5] by considering d-Cones, planar e-Cones and then conically confined e-Cones. The last one affords interaction of the types of constraint that may be imposed either at a material level as vertex angular excess or when forces are applied externally to cause a conical displacement field. Our approach is only valid for small deflections and rotations but has confirmed some of the known key dependencies when thinking about "output" measures of shape. In particular, we have seen that displacements (and fold rotations) do depend on the ratio of Gaussian charge to the square of indentation depth, and that we can produce the same displacement field by varying one or the other—in this sense, they become *interchangeable* [5]. A real benefit in our method is the use of the Gauss mapping, originally laid out in [13] for d-Cones. It provides direct and simpler insight into these constraint effects purely from a kinematical perspective; and being a vector method, any general mapping can be broken down into smaller stand-alone mappings, which define fundamental disclination effects. By focussing on these simpler elements, new insight into real and general disclination effects may be garnered, such as the singular properties at real vertices—which are not yet well understood. We have also seen the potential for gains in displacement capabilities by prescribing certain fold line layouts. In this sense, the structure behaves as a transducer of shape control with a single degree-of-freedom because four fold lines are needed to make the structure mobile; and we may, for example, drive rotations along one fold line using a motor, in order to produce displacements, and rotations, everywhere. Even though our analysis is restricted to small displacements, folded d-Cones are mobile for larger rotations because their layouts obey origami principles for folding their vertices flat. Folded e-Cones are strictly *kirigami* structures because material is added or removed by *cutting* before folding. However, we have chosen a fold line topology similar to d-Cones, which appears to allow flat-folding of e-Cones but we cannot be sure if there is some influence from the flexibility of the facets in our crude experiments. Hence, there may be common principles between origami and kirigami structures yet to be formally established.

References

[1] M Kleman and J Friedel. Disclinations, dislocations and continuous defects: a reappraisal. *Reviews of Modern Physics*, 80: 61-115, 2008.

[2] C R Calladine. Theory of Shell Structures. Cambridge University Press, 1983.

[3] M M Muller, M Ben Amar, and J Guven. Conical defects in growing sheets. *Physical Review Letters*, 101: 156104, 2008.

[4] J Chopin and A Kudrolli. Disclinations, e-Cones, and their interactions in extensible sheets. Submitted: http://arxiv.org/abs/1601.00575.

[5] E Efrati, L Pocivavsek, R Meza, K Y C Lee, and T A Witten. Confined disclinations: exterior vs material constraints in developable thin elastic sheets. *Physical Review E*, 91: 022404, 2015.

[6] E Cerda and L Mahadevan. Confined developable elastic surfaces: cylinders, cones and the Elastica. *Proceedings of the Royal Society A*, 461: 671-700, 2005.

[7] F Lechenault and M Adda-Bedia. Generic bistability in creased conical surfaces. *Physical Review Letters*, 115: 235501, 2015.

[8] S P Timoshenko and J M Gere. *Theory of Elastic Stability.* McGraw Hill, 1961.

[9] V Brunck, F Lechenault, A Reid, and M Adda-Bedia. Elastic theory of origami-based metamaterials. *Physical Review E*, 93: 033005, 2016.

[10] E Cerda and L Mahadevan. Conical surfaces and crescent singularities in crumpled sheets. *Physical Review Letters*, 80(11): 2358-2361, 1998.

[11] M Ben Amar and Y Pomeau. Crumpled paper. *Proceedings of the Royal Society A*, 453(1959): 729-755, 1997.

[12]] R J Lang. *The Complete Book of Origami.* Dover Publications, 1988.

[13] S M Farmer and C R Calladine. Geometry of "developable cones". *International Journal of Mechanical Sciences*, 47: 509-520, 2005.

[14] *ABAQUS Users Manual Version 6.11.* Dassault Systemes, Providence, RI, USA, 2011.

Figures

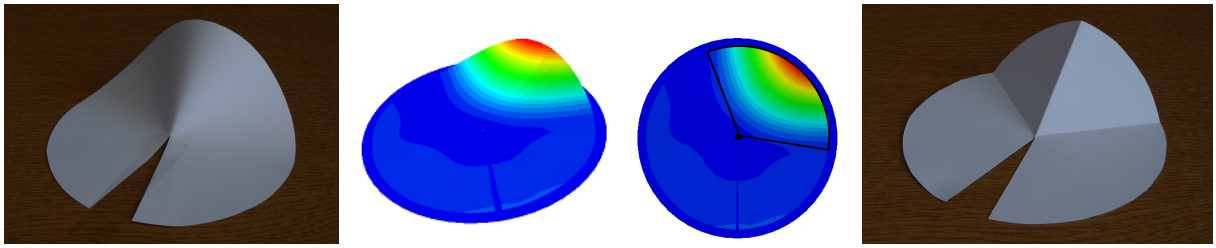

(a) (b) (c) (d)

Figure 1: The planar confined e-Cone. (a) A thin disk of paper card is cut radially and splayed open onto a flat surface. The deformed shape is held down by adhesive tape along the open edges. (b) and (c) Finite element analysis using the commercial software package ABAQUS [14]. A split disk made of elastic S4R5 shell elements sits slightly above a larger, rigid disk which performs as the underlying surface. A linear eigenvalue analysis of the elastic disk is performed to generate a stress-free transverse imperfection of 0.1%, in order to seed out-of-plane buckling as the split is opened, which is just visible. Zero friction contact between the two surfaces prevents interpenetration as the buckle moves away from the rigid base with differently coloured height contours; in (c), the outline wedge has been added to encapsulate transverse displacements larger than the initial imperfection, and subtends approximately 120°. (d) A discretely folded version of (a) using three fold lines symmetrically located with respect to the radial cut. The central fold line is a mountain fold, the other two are valley folds.

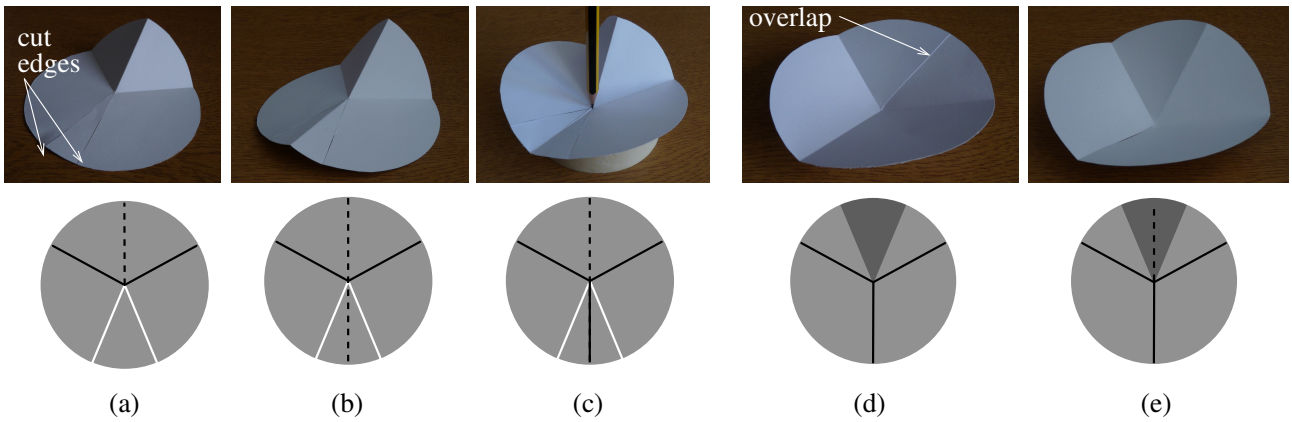

(a) (b) (c) (d) (e)

Figure 2: (a) The planar confined e-Cone of Fig. 1(d) with an added wedge of material in the open gap. (b) Like (a) except that the wedge has a central mountain fold forming a free-standing e-Cone. (c) A conically confined e-Cone formed by centrally loading the e-Cone of (b) sitting on a rim so that the wedge fold becomes a valley. (d) A stiff pyramid, or p-Cone, formed by cutting and overlapping a wedge of material. This has three symmetrical folds with the cut (and overlap) lying halfway between two of them. (e) Like (d) but with an extra valley fold for mobility. The row of schematic figures show valley folds as solid lines, mountain folds as dashed lines, material insertion (angular excess) as a white-bounded wedge, and material removal (angular deficit) as a darker wedge.

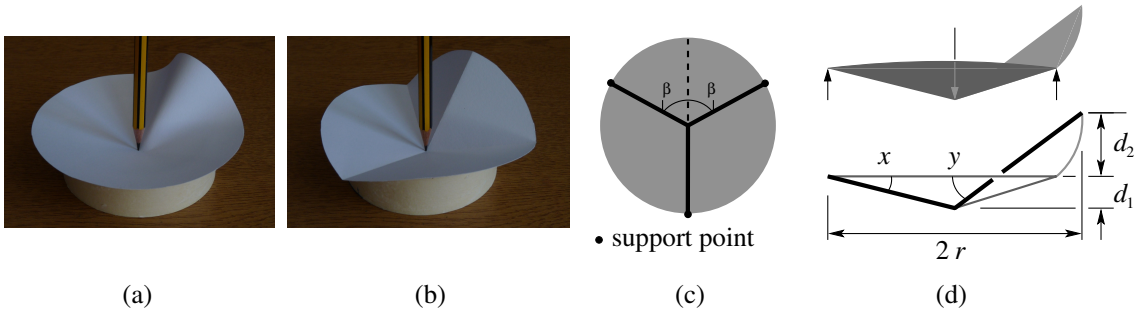

Figure 3: Deformation of a d-Cone. (a) Continuous d-Cone. (b) Discrete d-Cone. (c) Fold line layout for (b) where β is the half-width of the elevated portion above the rim. (d) Schematic side-view of the deformed discrete d-Cone showing the upward support forces and centrally applied downward force. The bottom sub-figure shows true views of the valley and mountain folds along the diameter in (c), which are rotated by angles x and y from the horizontal plane. The "conical indentation" from [5] is the displacement of the centre, d_1, and the upwards buckled displacement is d_2.

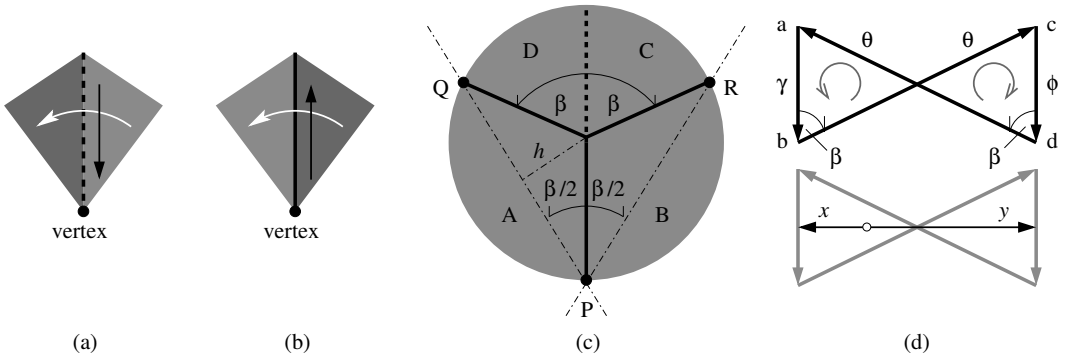

Figure 4: Kinematics of a discrete d-Cone. The direction of positive fold rotations as vectors along a mountain fold, (a), and valley fold, (b), when moving counter-clockwise around the vertex. (c) Like Fig. 3(c) but indicating the four facets A, B, C and D between fold lines, the three support points P, Q and R, and the support lines, PQ and PR. h is the perpendicular lever arm about PQ for calculating the displacement of the centre. (d) The Gauss mapping for the rotation vectors along the fold lines: $ab = \gamma$ pertains to a rotation, γ, between facets A and B, and so forth for θ (bc and da) and ϕ (cd). The internal curved arrows show the vector circuit when assessing the sign of the enclosed area. The bottom sub-figure shows how to relate x and y from Fig. 3(d).

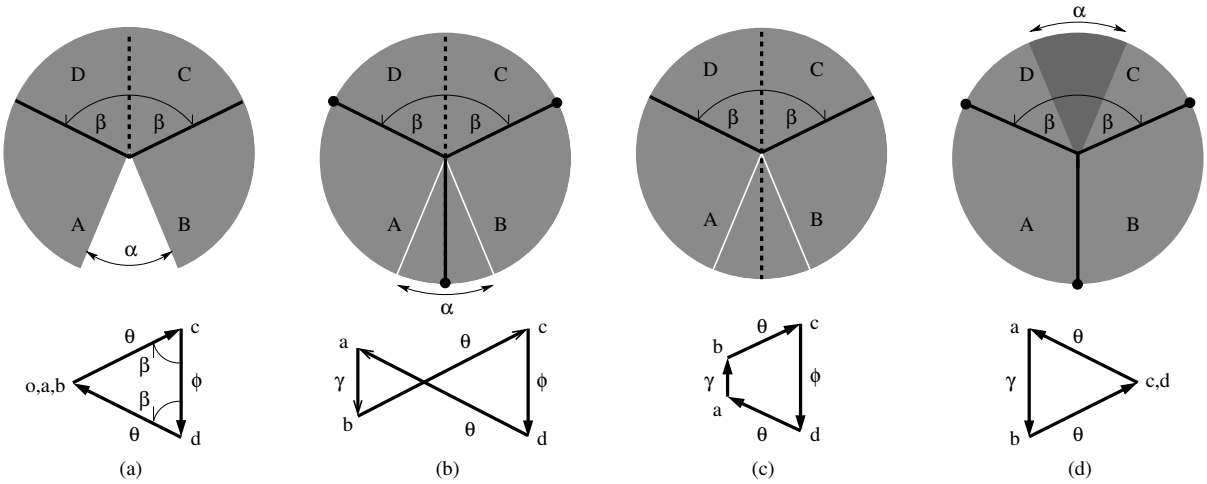

Figure 5: Gauss's mapping for the various folded shapes from Fig. 2. (a) The planar confined e-Cone. (b) The conically confined e-Cone. (c) The free-standing e-Cone. (d) The p-Cone. In all, the angular excess or deficit of the central vertex is of magnitude α. The fold notation and nomenclature are the same as in Figs 2 and 4.

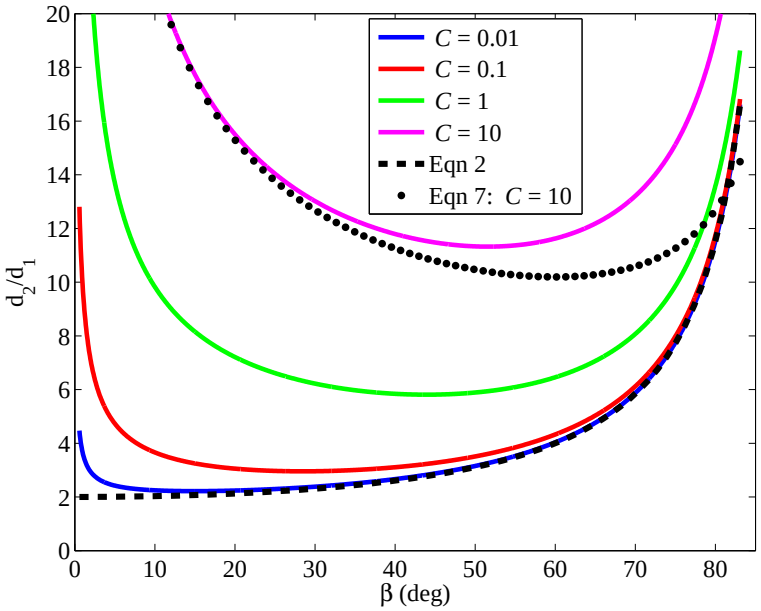

Figure 6: Discrete e-Cone displacements. C is equal to α/γ^2 and measures the influences of angular excess and conical indentation: a large value ($>> 1$) of C is close to the planar e-Cone case, Eqn 7, whilst a small value ($<< 1$) approaches d-Cone behaviour, Eqn 2. β can extend up to 90° but all curves rise asymptotically and diminish the earlier detail, hence the abscissa range as shown. The solid curves are exact solutions using Eqn 6.

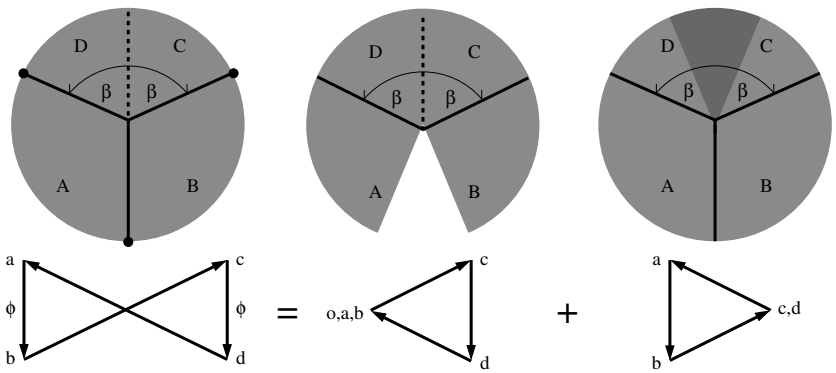

Figure 7: d-Cone properties from fundamental units. Gauss's mapping for a d-Cone, left, can be split into two cases of a planar e-Cone, middle, and a p-Cone, right, of equal and opposite angular excess and deficit, respectively.